SECED 2023 Conference
Earthquake Engineering & Dynamics for a Sustainable Future
14-15 September 2023, Cambridge, UK

BAYESIAN APPROACH OF SEISMIC RESPONSE OF RC WALLS WITH DUCTILE ELECTROWELDED REINFORCEMENT

Jorge E. EGGER[1], Christian MÁLAGA-CHUQUITAYPE[2],
Fabián R. ROJAS[3] & Leonardo M. MASSONE[4]

Abstract: *The response of reinforced concrete walls with two types of distributed reinforcement, namely, conventional reinforcement (A630) and ductile electrowelded reinforcement (A630S), is investigated. Taking as reference the results of 16 test on walls built with varied size and steel detailing, the main objective of this paper is to evaluate several hysteretic models for calibration, and compare their structural capacity, ductility, and strain distribution under cyclic loads. The findings show that both options produce significant strain levels (around 3% drift). Specimens prone to shear failure with electrowelded joints showed up to 20% lower displacement capacity but appreciable variability in ductility. No important differences are observed in terms of strength, and all specimens reached similar peak loads. Bayesian parameter identification is used in two hysteretic models (multilinear and Bouc-Wen) for each cycle. In general, the results show high accuracy in the parameter calibration after achieving 10 mm of lateral displacement.*

Introduction

The need for increased productivity, functionality, and quality is driving the construction sector towards safer solutions in seismic countries. Given the variety of material suppliers and building approaches aimed at increasing productivity, several options that can be taken to carry out a construction project in Chile and around the world. In this context, the use of ductile electrowelded reinforcement in reinforced concrete (RC) elements is an attractive alternative within the Chilean market. This technology allows short construction times and reduced alteration of the detailing of the reinforcement for concrete casting. However, electrowelded steel is distinctively less ductile than conventional steel. This aspect generates uncertainty and hampers its wider use in structural members, due to the potential implications under seismic events. However, a new steel material for electrowelded reinforcement has been developed to replicate the mechanical properties of A630 quality steel while allowing the bars to be welded.

To better describe the response of the above-mentioned structural elements with electrowelded reinforcement, it is necessary to analyse the parameters associated with their seismic hysteretic response. In this regard, nonlinear hysteretic systems are widely used in mechanical, aeronautics, geotechnical, and civil engineering fields. Nevertheless, an accurate description of the hysteretic response of a RC structure is complicated by the large uncertainties in their path-dependent relationship between deformation and resisting force. Since a dynamic analysis with a full-scale three-dimensional finite element model would demand high computational costs, many researchers have used an equivalent single-degree-of-freedom (SDOF) hysteretic system to represent a RC structure. The bilinear relationship model, in which the stiffness always returns to the original elastic stiffness upon load reversals and the strength remains unaffected by increases in inelastic strain or in the number of load reversals, has been considered a suitable idealization for behaviour of many structural elements. However, experimental as well as theoretical work on RC elements subjected to repeated and reversed loading have demonstrated that their post-yield behaviour is significantly different from the bilinear model. In such elements there is a loss of stiffness with cyclic increases in inelastic strain, even though there may be no apparent loss of strength. In 1970, Takeda et al. described a series of characteristics to be considered when building a multi-linear model, such as stiffness degradation in the hysteretic response (Takeda et al 1970). Other mathematical models that do not use multi-linear relationships have also been proposed in the previous scientific literature. In 1967, Bouc first proposed a hysteretic model in

[1] MSc student, Imperial College London, London, UK, jee22@ic.ac.uk
[2] Professor, Department of Civil and Environmental Engineering, Imperial College London, London, UK
[3] Professor, Department of Civil Engineering, University of Chile, Santiago, Chile
[4] Professor, Department of Civil Engineering, University of Chile, Santiago, Chile

differential form to simulate nonlinear cyclic systems, and a few years later, Wen modified this model by including smooth behaviour for structural random vibration analysis (Wen 1976).

There are various methods for parameter calibration of the models described above. Among them, the Bayesian approach has been gaining popularity recently, as it provides a rigorous framework to perform parameter identification and quantify the uncertainty of a model. This paper therefore compares the seismic behaviour of RC walls with electrowelded reinforcement using a simple multilinear hysteresis, and the original Bouc-Wen model to calibrate using Bayesian parameter identification as a tool for optimization. In contrast to previous literature, this work calibrates each parameter for each cycle, with the aim of seeing the evolution of the parameters and the parameter uncertainty as a function of the number of cycles. Additionally, photogrammetry results are included to be able to compare the response obtained from the tests with the failure modes.

Methodology

To obtain different failure modes and replicate multiple detailing configurations observed in Chilean constructions, a set of 16 RC wall specimens were built. In terms of geometry and detailing, 4 geometries are defined and described in Table 1 together with their corresponding notation, which is used throughout the remainder of the paper. The amount of reinforcing steel is quantified by ρ (the ratio of the area of reinforcement to the section area of the concrete member) also presented in Table 1, where ρ_l is the longitudinal reinforcement, ρ_t is the transverse reinforcement, and ρ_b is the stirrup contribution in the border elements. 4 specimens were built for each wall configuration. To study repeatability, 2 specimens are built with conventional steel (A630-420H), and the other 2 specimens are built with ductile electrowelded steel (A630-420HS) in the distributed reinforcement as shown in Figure 1. The difference between specimens with conventional reinforcement mesh “CM” and with ductile electrowelded mesh “EM” is mainly in the reinforcing steel curtain of the walls. Importantly, the mesh is only a part of the total reinforcement of the specimen, so the difference between the elements with CM and EM obey only to distinctions in their horizontal and vertical reinforcements. It is noteworthy that specimens with A630S ductile electrowelded mesh replicate the ties and bends used in the assembly of conventional steel. The variations in wall geometries are intended to capture the element behaviours for different slenderness values, thicknesses, and mesh quantities, incorporating flexural and shear failure modes. RC shear walls are conventionally classified into slender walls (H/L>3.0), moderate walls (1.5 ≤ H/L ≤ 3.0) and squat walls (H/L<1.5), where H is the wall height, L is the wall length, and t is the wall thickness.

Wall	H/L	t (m)	Horizontal/vertical mesh (curtain)	Confinement stirrups (between mesh)	Ties	Longitudinal border elements	ρ_l, ρ_t (%)	ρ_b (%)
W1	2.0	0.20	ϕ8@150mm (double)	1Eϕ8@150mm	ϕ8@150mm	2ϕ12	0.34	1.60
W2	1.0	0.20	ϕ8@200mm (double)	2Eϕ8@150mm	ϕ8@150mm	4ϕ12	0.25	1.30
W3	1.0	0.12	ϕ8@200mm (single)	2Eϕ8@150mm	-	4ϕ12+ϕ8	0.21	2.20
W4	1.0	0.12	ϕ8@120mm (single)	1Eϕ8@150mm	-	4ϕ12+ϕ8	0.35	2.20

Table 1. Detailing of RC walls.

(a) W1. *(b) W2.* *(c) W3.* *(d) W4.*

Figure 1. Wall reinforcement.

The strains developed in the walls are analysed using photogrammetry, a methodology used in attention to its low implementation cost, versatility, high precision, and the possibility of obtaining results that other sensors cannot detect, such as strain fields or crack patterns for the accurate identification of failure modes of the structural elements. Using this method, the data are recorded through a sequence of photographs by a camera, and these images are subsequently processed through specialized software. As a result, the displacement and strain fields on the surface of the element are obtained. In this work, the Ncorr software developed by Blaber et al. (2015) based on Digital Image Correlation (DIC) is used to output a strain matrix for each photograph examined. This allows the user to process the data in the most appropriate way.

Hysteretic models

Two mathematical models are used to represent the seismic response of RC walls with ductile electrowelded reinforcing steel: i) a multilinear (ML) model composed of straight lines (Figure 2.a), and ii) the original Bouc-Wen (BW) model (Figure 2.b).

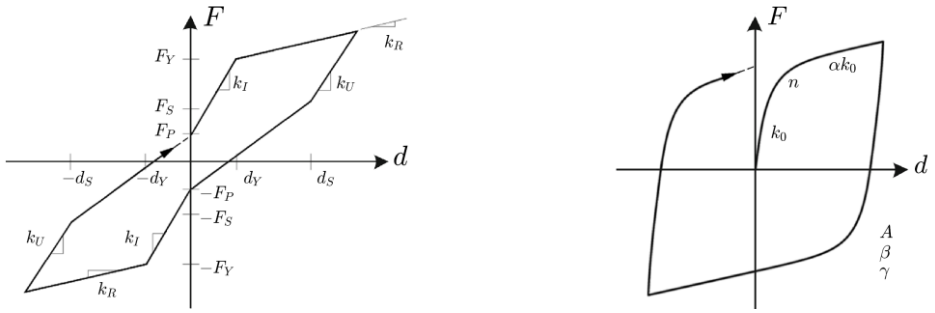

(a) Multilinear model. *(b) Bouc-Wen model.*

Figure 2. Hysteretic models.

The first hysteretic model is proposed based on prior experience and experimental results. Its parameters are: the initial stiffness k_I, stiffness degradation k_R, strength degradation after the ultimate load F_S, and pinching F_P. In addition, the original BW model is used. Despite the existence of other more sophisticated BW class models, the computational cost of the original model is much lower when optimizing the parameter selection. It should be mentioned that this work examines the evolution of the fitted parameters with each loading cycle, with the aim of gaining insight on their response and its associated uncertainty as a function of the number of cycles.

Nonlinear model updating

Bayesian parameter estimation approach

The mathematical models presented in this work have a certain number of unknown parameters whose values must be tuned using reliable data obtained from experimental tests, so that the simulated response of the system represents as accurate as possible the real response. This process is called identification, and it aims to evaluate the numerical values to be assigned to a vector collecting all the model parameters, named parameter vector θ. Let $\mathrm{y} = [\mathrm{y}_1, \ldots, \mathrm{y}_\mathrm{k}]$ denote the measured data obtained by the experimental testing, where k is the total number of time steps. In the context of this study's measurements in the laboratory, y refers to the lateral displacement of a RC wall specimen at the top under lateral cyclic loading.

The Bayesian approach for parameter estimation allows for a probabilistic point of view to be taken upon the values of model parameters. Its objective is to update prior beliefs about parameter values and variability through observed (or experimental) data and conditional probabilities, obtaining as an output the so-called posterior distribution (or posterior PDF) for each parameter. When conducting Bayesian batch estimation, the overall calibration of the model-predicted response with respect to observed data is considered. The derivation of this formulation stems from Bayes' theorem, which expressed in terms of observed response y, and model parameters θ yields Equation 1:

$$p(\theta|y) = \frac{p(y|\theta)\, p(\theta)}{p(y)} = \frac{1}{C} p(y|\theta) p(\theta) \tag{1}$$

Where $p(\theta|y)$ is the updated belief, commonly known as posterior PDF, about the values of parameters after measuring data y. The likelihood function $p(y|\theta)$ is related to the level of uncertainty associated to measured response y for given parameters θ. Prior distribution is represented by $p(\theta)$, which reflects the user's knowledge about θ in the absence of data, and $p(y)$, known as model evidence, is a multi-dimensional integral over an uncertain parameter space. The value of the evidence is known after the measurements are made, and the computation of this integral is often not practical. It is assumed here that the model evidence is a normalizing constant statistically independent of θ, and thus, it equals a constant number ($p(y) = C \in \mathbb{R}^+$). Equivalently, it is possible to omit the normalization constant C and express the unnormalized posterior density as:

$$p(\theta|y) \propto p(y|\theta)\, p(\theta) \tag{2}$$

In Bayesian estimation, the estimation of θ that maximizes the posterior PDF - i.e., the mode of $p(\theta|y)$ - is named the maximum a posteriori (MAP) estimation of θ:

$$\theta_{MAP} = \arg\max p(\theta|y) \tag{3}$$

It is usually more convenient to formulate the estimation problem as a minimization problem. Therefore, the MAP estimation of θ can be defined as:

$$\theta_{MAP} = \arg\min[-\ln p(\theta|y)] \tag{4}$$

$$\theta_{MAP} = \arg\min[-\ln p(y|\theta) - \ln p(\theta)] \tag{5}$$

When $p(\theta)$ is adequately flat and close to uniform, its natural logarithm converges to a constant value. Consequently, the MAP estimation problem expressed in Equation 3 simplifies into a maximum likelihood estimation (MLE) problem, formulated as:

$$\theta_{MLE} = \arg\min[-\ln p(y|\theta)] \tag{6}$$

Let $h = [h_1, \ldots, h_k]$denote the system output of the model with θ - i.e., the nonlinear response function - under the same excitation as the observed system output y. The measured output is modelled as:

$$\varepsilon_i(\theta) = y_i - h_i \tag{7}$$

In which $\varepsilon_i(\theta)$, the simulation error at the ith time step, encompass the discrepancy between the observed response of the structure and the model response. If the prediction error ε_i at different measured data points are independent and identically Gaussian distributed with zero mean and diagonal covariance matrix R, the likelihood function can be expressed as follows:

$$p(y|\theta) = \prod_{i=1}^{k} p(\varepsilon_i) \tag{8}$$

$$p(y|\theta) = \prod_{i=1}^{k} \frac{1}{(2\pi)^{n_\theta/2}|R|^{1/2}} \exp\left(-\frac{1}{2}[y_i - h_i(\theta)]^T R^{-1}[y_i - h_i(\theta)]\right) \tag{9}$$

$$p(y|\theta) = \frac{1}{(2\pi)^{n_\theta/2}|R|^{1/2}} \exp\left(-\frac{1}{2}\sum_{i=1}^{k}[y_i - h_i(\theta)]^T R^{-1}[y_i - h_i(\theta)]\right) \tag{10}$$

Where $|R|$ denotes the determinant of the diagonal covariance matrix R, and n_θ denotes the number of parameters to be identified. The diagonal entries of the covariance matrix R are piled in a row vector called the simulation error variance vector, where r_j denotes the jth diagonal entry of R matrix ($|R| = \sum_{j=1}^{n_\theta} r_j$). The objective function of the optimization problem is then given by:

$$J(\theta) = -\ln p(y|\theta) \tag{11}$$

$$J(\theta)=\frac{kn_\theta}{2}\ln 2\pi+\frac{k}{2}\sum_{j=1}^{n_\theta}\ln r_j+\frac{1}{2}\sum_{j=1}^{n_\theta}\sum_{i=1}^{k}\frac{\left[y_i-h_{ij}(\theta)\right]^2}{r_j} \tag{12}$$

Following Equation 6, the extended estimation problem can be defined as the following optimization problem:

$$\hat{\theta}=\arg\min J(\theta) \tag{13}$$

The most probable value $\hat{\theta}$ is determined by minimizing $J(\theta)$ in Equation 13, which requires the computation of the gradient vector of the objective function with respect to the estimation parameters. The nonlinear optimization problem formulated in Equations 12 and 13 can be solved through gradient-based optimization methodologies, such as the conventional least-squares method for parameter estimation. The computational optimization algorithm available as part of the MATLAB optimization toolbox is used herein.

Parameter estimation uncertainty quantification

Parameter uncertainty is usually described by a covariance matrix. The covariance matrix estimation result can be asymptotically converged to the Cramér-Rao lower bound (CRLB). The CRLB is often calculated using the Fisher information matrix (FIM) denoted as $I(\theta,r)$.

$$I(\theta,r)=\begin{bmatrix}I_{\theta\theta} & 0\\ 0 & I_{rr}\end{bmatrix} \tag{14}$$

where $I_{\theta\theta}$ and I_{rr} are sub-matrices. In this case, the hysteretic model parameter vector θ present time-invariant unknown parameters, which are modelled as random variables denoted by Θ. Considering that the FIM is a block matrix defined by expectations $E\{\cdot\}$, the CRLB for the covariance matrix is often computed as:

$$\mathrm{Cov}(\Theta)\geq {I_{\theta\theta}}^{-1} \tag{15}$$

Therefore, the sub-matrix $I_{\theta\theta}\in\mathbb{R}^{n_\theta\times n_\theta}$ can be written as:

$$I_{\theta\theta}=E\left\{\left(\frac{\partial \ln p(y|\theta)}{\partial\theta}\right)^T\left(\partial\ln p\left(\frac{y|\theta}{\partial\theta}\right)\right)\right\}_{\text{at }\theta,r} \tag{16}$$

$$I_{\theta\theta}=E\left\{\sum_{i=1}^{k}\left[\left(\frac{\partial h_i(\theta)}{\partial\theta}\right)^T R^{-1}\left(y_i-h_i(\theta)\right)\right]\sum_{j=1}^{k}\left[\left(y_j-h_j(\theta)\right)^T R^{-1}\left(\frac{\partial h_j(\theta)}{\partial\theta}\right)\right]\right\}_{\text{at }\theta,r} \tag{17}$$

$$I_{\theta\theta}=\sum_{i=1}^{k}\sum_{j=1}^{k}\left[\left(\frac{\partial h_i(\theta)}{\partial\theta}\right)^T R^{-1}E\left[\left(y_i-h_i(\theta)\right)\left(y_j-h_j(\theta)\right)^T\right]R^{-1}\left(\frac{\partial h_j(\theta)}{\partial\theta}\right)\right]_{\text{at }\theta,r} \tag{18}$$

$$I_{\theta\theta}=\sum_{i=1}^{k}\left[\left(\frac{\partial h_i(\theta)}{\partial\theta}\right)^T R^{-1}\left(\frac{\partial h_i(\theta)}{\partial\theta}\right)\right]_{\text{at }\theta,r} \tag{19}$$

It can be shown that the FIM is equal to the negative of the expected value of the Hessian matrix of the log-likelihood function evaluated at the true value of the vectors θ, r. It is worth noting that $\hat{\theta}$ and $\hat{r}$ converge asymptotically to θ and r, respectively, and therefore, the parameter estimation covariance matrix asymptotically converges to the CRLB computed at $\hat{\theta}$ and $\hat{r}$. The diagonal entries are used to describe the variance of the estimated parameters. Assuming that the obtained covariance matrix usually has nonzero off-diagonal entries, and these entries may have a significant influence, the Schur complement method provides an effective way to calculate the variance of each individual parameter (Cao et al 2019). If the model parameter vector θ is partitioned in two parts $\theta=[\theta_1^T\theta_2^T]$, the $I_{\theta\theta}$ matrix is partitioned in four blocks as:

$$I_{\theta\theta}=\begin{bmatrix}I_{11} & I_{12}\\ I_{21} & I_{22}\end{bmatrix} \tag{20}$$

Finally, the CRLB of the covariance matrix of the estimation of θ_1 can be found using the generalized Schur complement of I_{11} in $I_{\theta\theta}$:

$$\mathrm{Cov}(\Theta_1) \geq \left(\mathrm{I}_{11} - \mathrm{I}_{12}\mathrm{I}_{22}{}^{-1}\mathrm{I}_{21}\right)^{-1} \quad (21)$$

In the presence of a single realization of the experimental response data, the expectation operation can be dropped and the FIM can be approximated by the negative of the Hessian of the log-likelihood function. For such MLE optimization algorithms, computing the FIM using the Hessian matrix at the converged optimal point would be at no additional computational cost.

Results and analysis

Experimental response

Figure 3 shows the lateral load versus lateral top displacement of the specimens under study. W1 specimens show an evident regularity in the results achieved for their 4 elements, both in terms of strength and strain. A maximum drift of 2.97% and a capacity of 213 kN are achieved. Their nominal capacity is 151 kN. In both cases (CM and EM), the displacements are achieving a percentage of approximately 80% of the total drift. This means that the structural capacity of the element is determined by the vertical reinforcement, with a significant participation from the ϕ12 mm diameter lining located in the border elements together with the distributed mesh. For the W2 specimens, similarity results are obtained. The maximum drift recorded is 2.96% and the strength is 719 kN. Their nominal capacity is 553 kN. In both cases, the displacements are achieving a percentage of approximately 70% of the total drift. This means that although the structural behaviour of the element is strongly influenced by the performance of the boundary reinforcement, the double curtain demonstrates a greater participation in the resistance than in W1 specimens. In the case of W3 specimens, the CM response also has a slightly higher ductility than the EM. The maximum drift recorded is 2.06% and their capacity is 569 kN. The nominal capacity is 412 kN. The peak displacement recorded in the EMA and EMB is approximately 20% less than that of the CMA and CMB specimens. The W4 specimens register incipient differences in ductility, where the structural elements built with conventional reinforcement achieve slightly higher displacements (differences close to 20%), managing to complete a greater number of cycles for a given displacement level. The maximum drift recorded is 2.26% and the capacity is 564 kN. The nominal load is 433 kN. The responses show that reducing the wall thickness reduces their ductility and capacity compared to those illustrated in thicker wall responses. Lateral load degradation is also observed to be faster once the capacity is achieved, but in general, these specimens present similar ductility characteristics.

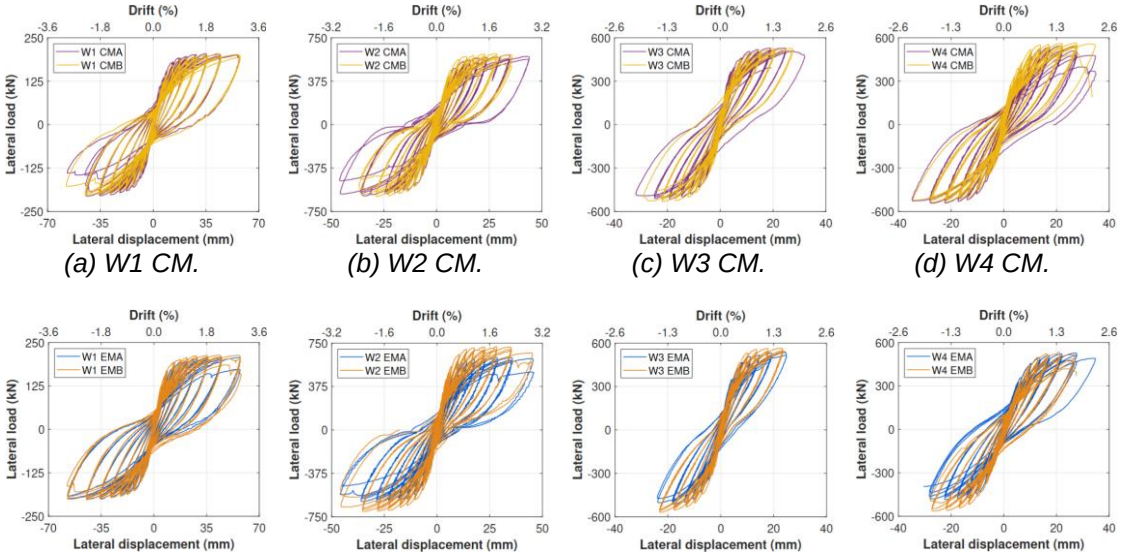

(a) W1 CM. *(b) W2 CM.* *(c) W3 CM.* *(d) W4 CM.*

(e) W1 EM. *(f) W2 EM.* *(g) W3 EM.* *(h) W4 EM.*

Figure 3. Experimental response of RC walls with conventional mesh (CM) and electrowelded mesh (EM).

Bayesian identification of multilinear model

The parameter vector of the multilinear hysteretic model to be identified using the Bayesian approach is $\theta = [d_Y, d_S, F_Y, F_S, F_P]$, where $k_I = F_Y/d_Y$ and k_R, k_U can be obtained using the optimized parameters. A direct calibration of the slopes is not considered in the parameter vector to make the Bayesian problem identifiable. The maximum displacement d_U and the ultimate load of the RC wall response F_U can be directly determined from the test data. Figure 4 shows examples of fitted curves using the proposed multilinear model, while Figure 5 shows the parameter evolution over number of cycles for walls W1 using Bayesian estimation. It is observed from these figures that the hysteretic curves capture very well the parameters of displacement and strength. The parameters observed in Figure 5 tend to increase with the number of cycles for the 5 calibrated parameters, particularly for displacements and pinching strength. Yield strength and degradation strength increase after ultimate load, and then remain constant afterwards (between cycles 10 and 20 approximately) until wall failure. The uncertainty in the calibrated parameters, represented in this case as the diagonal values of the covariance σ, presents the highest values at the beginning of the tests for all RC walls, reducing drastically afterwards and tending to zero as observed in the examples of Figure 6. This is because the measured data is imprecise for displacements of less than 10 mm in the first cycles.

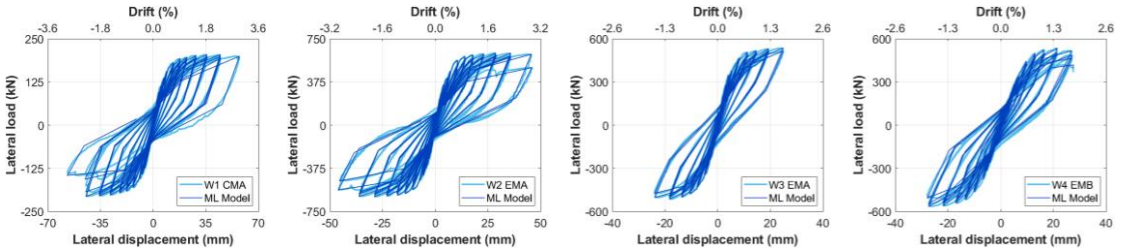

(a) W1 CMA. *(b) W2 EMA.* *(c) W3 EMA.* *(d) W4 EMB.*

Figure 4. Measured and fitted hysteretic curves using multilinear model.

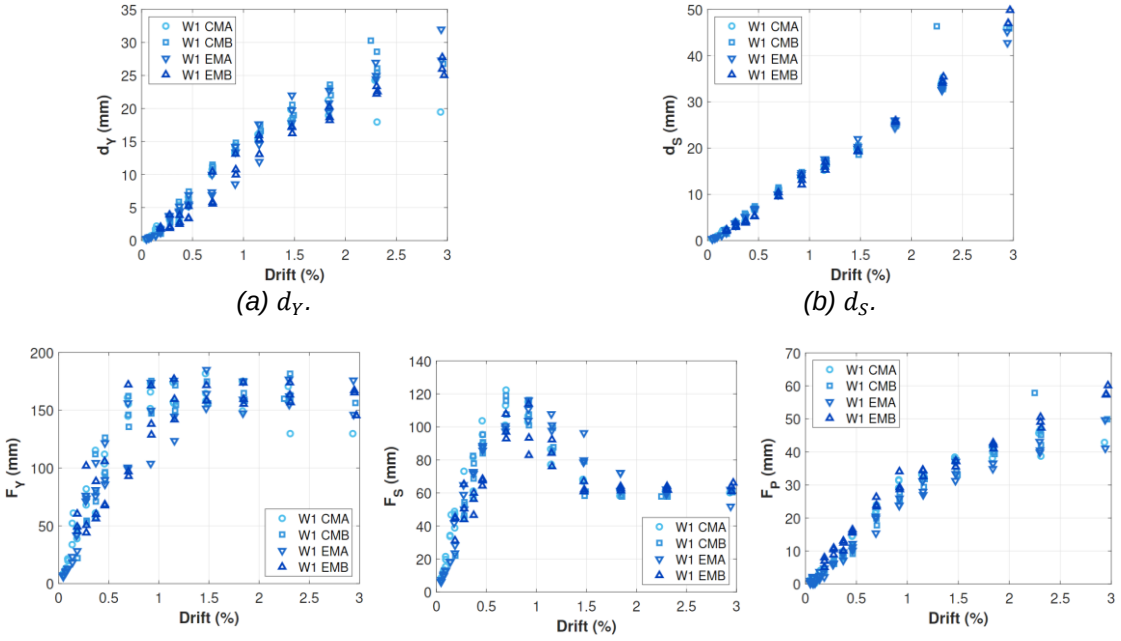

(a) d_Y. *(b) d_S.*

(c) F_Y. *(d) F_S.* *(e) F_P.*

Figure 5. Bayesian parameter identification of W1 using multilinear model.

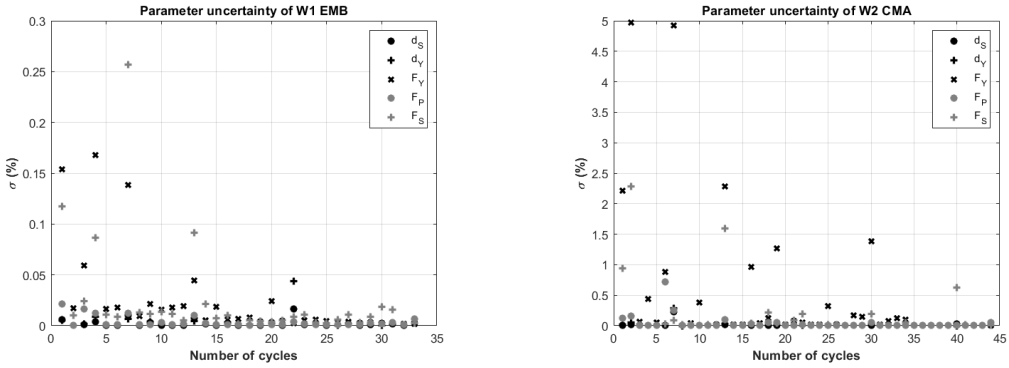

(a) W1 EMB. *(b) W2 CMA.*

Figure 6. Examples of variance evolution for each cycle using multilinear model.

Bayesian identification of Bouc-Wen model

The parameter vector of the original BW hysteretic model to be identified using Bayesian approach is $\theta = [A, \beta, \gamma, n, \alpha, k_0]$. Figure 7 shows examples of fitted curves using the proposed BW model, while Figure 8 shows the evolution of parameter values over number of cycles for walls W4. The hysteretic responses are well-fitted, however there is a low accuracy in the curve close to the pinching zone and the strength degradation. This is because the original BW model does not incorporate these variables. The parameters presented as examples in Figure 8 show a tendency towards the zero value in most of the tested walls W4. In general, the uncertainty evolution in the calibrated parameters presents higher values than those observed in the multilinear model, as depicted in the examples of Figure 9. This is attributed to the fact that the BW class model does not incorporate essential parameters that allow the response to be better modelled, such as pinching or strength degradation. This also implies a higher computational cost for Bayesian identification in terms of convergence.

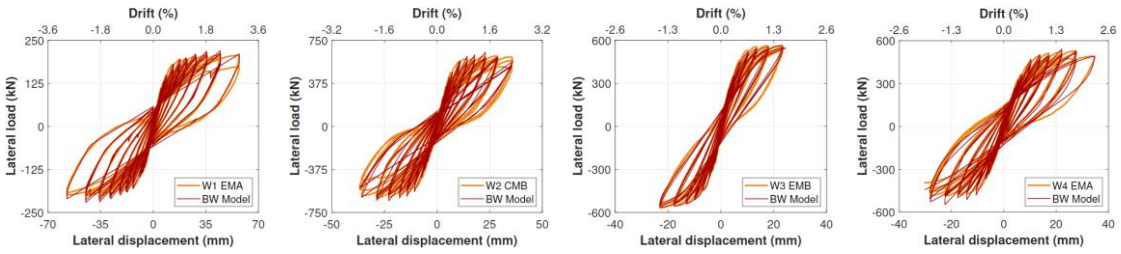

(a) W1 EMA. *(b) W2 CMB.* *(c) W3 EMB.* *(d) W4 EMA.*

Figure 7. Measured and fitted hysteretic curves using Bouc-Wen model.

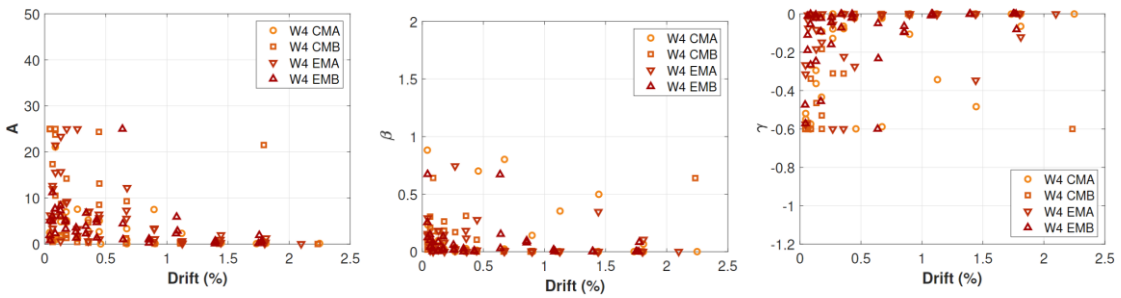

(a) A. *(b) β.* *(c) γ.*

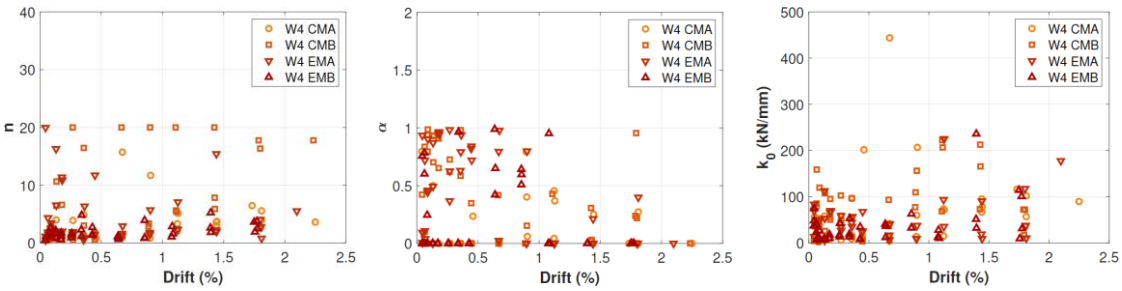

(c) n. *(d) α.* *(e) k_0.*

Figure 8. Bayesian parameter identification of W4 using Bouc-Wen model.

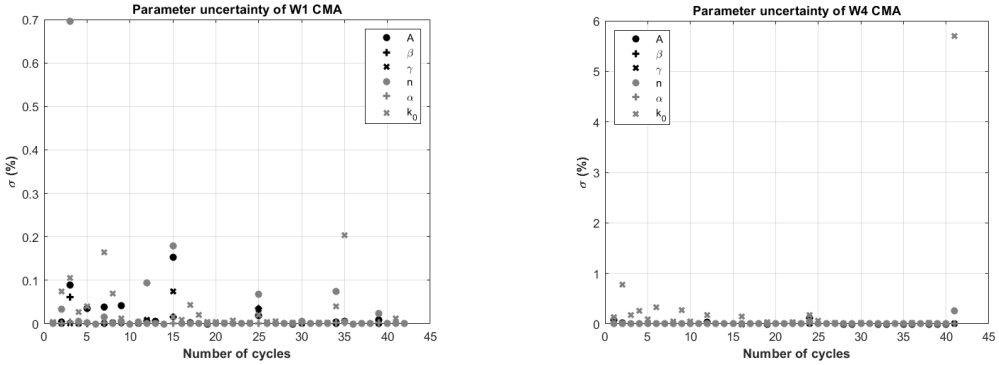

(a) W1 CMA. *(b) W4 CMA.*

Figure 9. Examples of variance evolution for each cycle using Bouc-Wen model.

Photogrammetric results

Figure 10 illustrates that the slender walls W1 and W2 show a concentration of vertical strains ε_{yy} at the base of the structural element, where the greatest strains of the longitudinal bars also occur in the same area where concrete detachment is observed during the test. Regarding its respective experimental and fitted hysteretic response of W1 and W2 specimens, a maximum total drift of approximately 3% is reached. This implies that the failure of slender RC walls is conditioned by flexure, which coincides with that obtained by DIC. In contrast, walls W3 and W4, with maximum total drifts between 2% and 2.3% respectively, show diagonal failures on the front surface of the structural element observed by horizontal strains ε_{xx}. Additionally, the work by Massone et al. (2021) concludes that the relationship between the horizontal strain ε_{xx} and the shear strain γ_{xy} is slightly nonlinear in RC panels. Thus, this implies that the squat RC walls are conditioned by the shear stress in relation to the behaviour of the horizontal expansion observed by DIC. Finally, failure modes observed by photogrammetry are properly well fitted using both models, which implies that Bayesian approach can calibrate flexural and shear components.

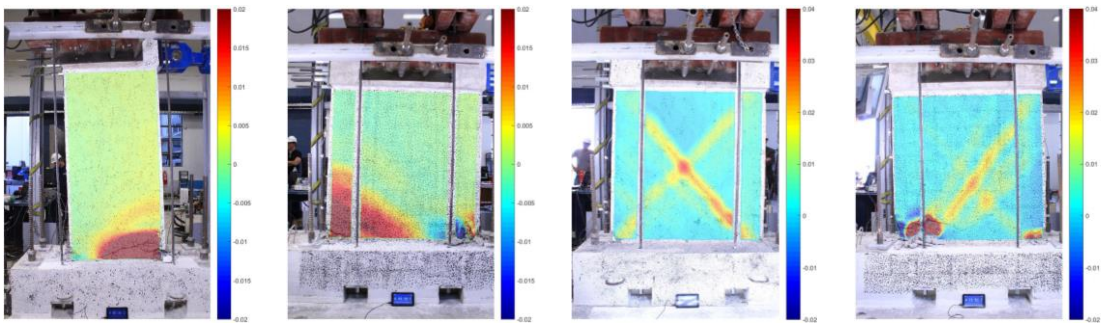

(a) W1 EMB (ε_{yy}). Drift = -3.0%. *(b) W1 EMB (ε_{yy}). Drift = +3.0%.* *(c) W3 EMA (ε_{xx}). Drift = +1.6%.* *(d) W4 EMB (ε_{xx}). Drift = -1.8%.*

Figure 10. Strain fields of RC walls.

Conclusions

A set of 16 specimens consisting of RC walls with conventional steel and ductile electrowelded mesh was examined in this paper. A description of some of the experimental findings and measurements made is provided below:

- The experimental results show that the response of the structure is only marginally influenced by the type of steel used in the mesh (i.e., whether conventional steel CM A630-420H, or ductile electrowelded steel EM A630-420HS is used). Although the observed differences affect their ductility, both solutions have significant deformation capacities, where the serviceability of the structure is not altered. This means that the differences in ductility (approximately 20% lower in the EM solution) are evident after important damage has already taken place on these elements, e.g., from 1.3% drift for W3 and 1.8% for W4, when their yield values are approximately 0.6% and 0.8%, respectively. The double curtain is applied mainly as vertical reinforcement (consistent with the crack patterns) and, in general, no appreciable damaged was observed in this area. The interference of the mesh in the capacity of the elements gradually increases in specimens W2 and W4.
- A Bayesian approach is employed to identify the parameters of a multilinear model and a BW model. The calibrated samples showed good agreement with a wide range of collected data, and a good agreement was also observed between the hysteretic parameters of the models and test results. The parameters of the ML model show an increase in their values as the cycles increase, and their uncertainty decreases and tending to zero until failure. In contrast, the parameters of the BW model generally remain constant during the experimental test, however, its uncertainty is slightly greater than that of the ML model. This is because parameters, such as pinching or strength degradation, are not incorporated into the latter model, so the fit with the data curve is less accurate.
- Contrary to conventional sensors, photogrammetry allows strain distributions and failure patterns of RC elements to be observed directly. For slender walls dominated by flexure, it is observed that the strain concentration is located at the wall boundaries. In contrast, diagonal failure modes are observed on the panel for squat walls conditioned by shear. It is noteworthy that flexure and shear failures observed by DIC are highly well captured by Bayesian parameter identification, which means that the models can calibrate both failure responses.

References

Blabler J, Adair B and Antoniou A (2015), Ncorr: Open-Source 2D Digital Image Correlation Matlab Software, *Experimental Mechanics*, 55(6): 1105–1122

Cao J, Xiong H, Chen J and Huynh A (2019), Bayesian parameter identification for empirical model of CLT connections, *Construction and Building Materials*, 218: 254–269

Ebrahimian H, Astroza R, Conte JP and Papadimitriou C (2018), Bayesian optimal estimation for output-only nonlinear system and damage identification of civil structures, *Structural Control Health Monitoring,* 25(4), e2128

Ebrahimian H, Astroza R, Conte JP and de Callafon, RA (2017), Nonlinear finite element model updating for damage identification of civil structures using batch Bayesian estimation, *Mechanical Systems and Signal Processing,* 84, 194-222

Massone L, López C and Kolozvari K (2021), Formulation of an efficient shear-flexure interaction model for planar reinforced concrete walls, *Engineering Structures*, 243: 112680

Takeda T, Sozen M and Nielsen N (1970), Reinforced concrete response to simulated earthquake, *Journal of the Structural Division*, 96(12)

Wen Y (1976), Method for random vibration of hysteretic systems, *Journal of the Engineering Mechanics Division, ASCE*, 102(2): 249-263